Symmetries and transport in site-dependent driven quantum lattices

Thomas Wulf,[1,*] Christoph Petri,[1] Benno Liebchen,[1] and Peter Schmelcher[1,2,†]
[1]*Zentrum für Optische Quantentechnologien, Universität Hamburg, Luruper Chaussee 149, 22761 Hamburg, Germany*
[2]*The Hamburg Centre for Ultrafast Imaging, Universität Hamburg, Luruper Chaussee 149, 22761 Hamburg, Germany*
(Received 18 August 2014; published 17 October 2014)

We explore the quantum dynamics of particles in a spatiotemporally driven lattice. A powerful numerical scheme is developed which provides us with the Floquet modes and thus enables a stroboscopic propagation of arbitrary initial states. A detailed symmetry analysis represents the cornerstone for an intricate manipulation of the Floquet spectrum. Specifically, we show how exact crossings can be converted into avoided ones, while the widths of these resulting avoided crossings can be engineered by adjusting parameters of the local driving. Asymptotic currents are shown to be controllable over a certain parameter range.

DOI: 10.1103/PhysRevE.90.042913 PACS number(s): 05.45.Mt, 05.60.Gg, 03.75.Kk

I. INTRODUCTION

Periodically driven systems which allow for the extraction of work out of an unbiased environment are often termed "ratchets." Because originally these systems relied on the rectification of thermal noise they were seen as realizations of Brownian motors, the corresponding research field being highly active (see [1] and references therein). Experimentally, ratchet physics has been explored in a variety of different setups such as crystals exposed to intense laser fields [2] or cold atoms loaded into driven optical lattices, and the latter have proven to be particularly insightful since they allow for a precise control over the system parameters [3–7]. While some of these experiments are carried out at moderate temperatures and allow for a classical treatment [3–5], others could reach ultracold temperatures and demonstrated the accessibility of Hamiltonian ratchet setups operating deep in the quantum regime [6,7]. The experimental advances concerning these newly realized "quantum ratchets" were accompanied by a substantial body of theoretical work (see [8–16] and references therein). Thereby, one of the main achievements was the classification of the symmetries which need to be broken in order to allow for the observation of a ratchet current [17]. Besides that, the discussed phenomena associated with quantum ratchets were manifold. Examples are the existence of resonances in the directed current [12,18], the possibility of tuning the dispersion rate of a wave packet [19], or the harvesting of Landau-Zener transitions [20]. Another active subarea of ratchet physics are periodically kicked systems, which have the advantage of being more accessible from a theorist's point of view due to the simpler δ-shaped time dependence. In these, similar effects as for the aforementioned smoothly driven setups could be observed, such as directed transport, resonance behavior, and even the acceleration of ratchet currents [21–25].

In any case, all of the aforementioned works related to ratchet physics, be it classical, quantum, smoothly driven, or kicked, are restricted to globally acting driving forces. Over recent years, however, for classical particles loaded into driven lattices, it was shown that a site-dependent driving can add to the already existing diversity of physical phenomena in ratchet setups [26–32]. In [26] for example it was shown how a protocol based on a site-dependent driving leads to the patterned deposition of particles out of a uniform initial particle distribution. Furthermore, [27–29] demonstrated the possibility for particles to undergo conversion processes from diffusive to regular motion, something explicitly forbidden for globally uniform driving forces and which leads to a plethora of nonequilibrium phenomena for the dynamics. Inspired by these interesting observations, it seems an intriguing perspective to carry over the idea of a spatially nonglobal driving from the classical setups to the realm of quantum ratchets. This is precisely the purpose of this work. An additional motivation for this project is the development of cold atom experiments which also deviate from the simple case of a spatially uniform driving force. A noteworthy idea in this context is the introduction of subwavelength lattices [33] which allow for the construction of more complicated unit cells of the lattice. Full control over each of the lattice barriers is achieved in experiments with so-called "painted potentials" [34], even though these are until now restricted to just a few barriers and do not yet consider extended lattices.

In the present paper we show that for a quantum particle exposed to a periodically oscillating lattice, the inclusion of a site-dependent driving indeed leads to interesting phenomena. Such setups are investigated here in the framework of Floquet-Bloch theory, and we demonstrate how, by breaking the translational invariance through the local driving, a set of different symmetry classes for the Floquet-Bloch modes evolves. This is demonstrated to have significant impact on the Floquet spectrum where we observe the transformation from exact to avoided crossings for a deviation from global towards a site-dependent driving. Even more, we find that the width of the resulting avoided crossing is controllable through variation of a single parameter of the local driving. This is particularly interesting, because the width of avoided crossings in Floquet spectra of driven lattices is of relevance for a variety of physical phenomena, two noteworthy examples being the already mentioned Landau-Zener transitions [18] or quite generally the diffusion properties of a wave packet [35]. Finally, we show the possibility of a directed current in our system, even for the case where all individual barriers do not

*Thomas.wulf@physnet.uni-hamburg.de
†Peter.Schmelcher@physnet.uni-hamburg.de

break the relevant symmetries. Consequently, the symmetry breaking becomes a collective phenomenon of the barriers constituting the lattice.

This work is structured in the following way: In Sec. II we introduce the setup of the spatiotemporally driven lattice. In Sec. III we show how a well-known scheme to calculate the time evolution operator in a periodically driven system can be extended in order to simulate the time evolution in a site-dependent driven lattice. In doing so, we also take the possibility of nonzero quasimomenta into account. In Sec. IV we perform a thorough symmetry analysis and identify symmetry classes for the Floquet-Bloch modes, which arise due to the site-dependent driving. In Sec. V we show how the existence of these symmetry classes is translated into properties of the Floquet spectrum. Section VI contains an investigation of the transport properties of our setup. Finally, we conclude and provide an outlook in Sec. VII.

II. THE SPATIOTEMPORALLY DRIVEN LATTICE

The system under investigation consists of a single quantum particle in one dimension exposed to a laterally oscillating lattice of Gaussian potential barriers. Hence the dynamics obeys the time-dependent Schrödinger equation (TDSE)

$$i\hbar\frac{\partial\Psi(x,t)}{\partial t} = H(x,t)\Psi(x,t), \tag{1}$$

where x and t denote position and time and the Hamiltonian is given by

$$H(x,t) = -\frac{\hbar^2}{2m}\frac{\partial^2}{\partial x^2} + V_0\sum_{s=-\infty}^{\infty} e^{-[x-sL-d_s(t)]^2/\Delta^2}. \tag{2}$$

Here, Δ, L, m, and V_0 are the barrier width, the distance between the barriers' equilibrium positions, the particle mass, and the height of the potential barriers, respectively, while $d_s(t)$ is the driving law. Without loss of generality we will set $m = \hbar = 1$ in the following. The crucial difference from Hamiltonians usually studied in investigations of driven lattices in the quantum regime is that the driving law carries a barrier index s and thus can be site dependent. Throughout this work, we employ a cosine driving with equal amplitude and frequency but with possibly different phases:

$$d_s(t) = A\cos(\omega t + \delta_s). \tag{3}$$

Moreover, we restrict ourselves to sequences of the barrier phases which periodically repeat themselves after some number of barriers n_p, i.e., we have $\delta_s = \delta_{s+n_p}$. Because of the intimate relation between the driving of a lattice site and its barrier index s, and thus its position within the lattice, we call a setup with $n_p > 1$ a spatiotemporally driven lattice. In contrast, for the case of only a single employed driving law, i.e., $n_p = 1$, we say the lattice is uniformly driven. A sketch of a spatiotemporally driven lattice for the case of three different driving laws ($n_p = 3$) is shown in Fig. 1.

In principle one could also imagine more complicated unit cells containing more barriers or even more complicated driving laws. The only restrictions that we have to make in order to employ the computational scheme as presented in the following section are that the Hamiltonian remains periodic in time and that two neighboring barriers do not have a notable overlap at any time.

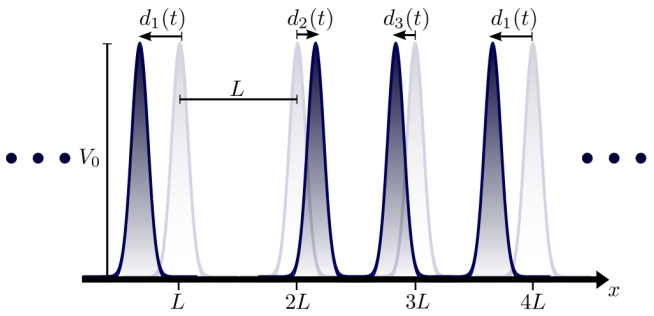

FIG. 1. (Color online) Snapshot of a spatiotemporally driven lattice consisting of Gaussian barriers of height V_0 with lattice spacing L. Three different driving laws $d_s(t)$ for $s = 1,2,3$ are periodically repeated. The shaded barriers indicate the equidistant equilibrium positions of the barriers.

III. COMPUTATIONAL SCHEME: THE PROPAGATOR METHOD

In this section we develop a computational scheme in the framework of Floquet-Bloch theory which enables us to propagate an arbitrary initial state according to the Hamiltonian given by Eq. (2). Our formalism is based on the ideas presented in [36] (see also [37]), and was originally designed to study atomic and molecular multiphoton processes. In the following, we show how the formalism can be extended in order to describe the dynamics in a spatiotemporally driven lattice as introduced in the previous section. In doing so, we have incorporated the possibility of a nonzero quasimomentum as well as the complex nature of the unit cell which can contain several barriers, each equipped with a different driving law.

Other ideas as to how Floquet and Bloch theory can be applied simultaneously to study temporally and spatially periodic systems have been developed earlier in order to investigate solids which are exposed to intense laser fields, for example in the context of higher harmonic generation [38]. However, the computational schemes employed in these works are tailored towards globally acting ac forces and cannot easily be adapted to systems with spatially varying driving forces, such as the spatiotemporally driven lattice.

A. Floquet-Bloch theory

To be self-contained, let us start by summing up the most important results from Floquet and Bloch theory. Because the Hamiltonian under investigation is periodic in time with $H(x,t) = H(x,t+T)$ and $T = \frac{2\pi}{\omega}$, Floquet's theorem ensures that every solution of Eq. (1) can be written as

$$\Psi_\alpha(x,t) = e^{-i\epsilon_\alpha t}\Phi_\alpha(x,t), \tag{4}$$

where the Floquet mode (FM) Φ_α respects the periodicity of the Hamiltonian, i.e., $\Phi_\alpha(x,t) = \Phi_\alpha(x,t+T)$, and ϵ_α is a real number often termed the "quasienergy" (QE). It is straightforward to see that adding or subtracting some integer multiple of ω to the QE while simultaneously multiplying the FM by an appropriate phase factor leaves the solution of the

TDSE $\Psi_\alpha(x,t)$ invariant. Hence, the QEs can always be chosen to be within the interval $[-\frac{\omega}{2}, \frac{\omega}{2}]$.

Knowing the FMs of our system is of particular relevance because it allows us to compute the time evolution of any initial state. This is because they are eigenstates of the time evolution operator $U(t,t_0)$ over one period of the driving:

$$U(T+t_0,t_0)\Phi_\alpha(x,t_0) = e^{-i\epsilon_\alpha T}\Phi_\alpha(x,t_0), \tag{5}$$

which follows directly from applying the time evolution operator $U(T+t_0,t_0)$ to the solution of the TDSE $\Psi_\alpha(x,t)$. Hence, the stroboscopic time evolution of an arbitrary initial state can be calculated as [11]

$$\Psi(x,mT+t_0) = \sum_\alpha C_\alpha(t_0)e^{-i\epsilon_\alpha mT}\Phi_\alpha(x,t_0), \tag{6}$$

where the $C_\alpha(t_0)$ are obtained as the overlap of the initial state with the FM $\Phi_\alpha(x,t_0)$. So far we have taken into account only the temporal periodicity of our system. However, the Hamiltonian considered in this work features spatial periodicity as well, since $H(x,t) = H(x+n_pL,t)$. Accordingly, the FMs can be written in terms of Floquet-Bloch modes (FBMs) as $\Phi_{\alpha,\kappa}(x,t) = e^{i\kappa x}\phi_{\alpha,\kappa}(x,t)$ with $\phi_{\alpha,\kappa}(x,t) = \phi_{\alpha,\kappa}(x+n_pL,t) = \phi_{\alpha,\kappa}(x,t+T)$ and $\kappa \in [-\pi/(n_pL), +\pi/(n_pL)]$ being the quasimomentum. The stroboscopic time evolution for an initial state [Eq. (6)] becomes then [11]

$$\Psi(x,mT+t_0) = \int_{-\pi/(n_pL)}^{+\pi/(n_pL)} d\kappa \sum_\alpha C_{\alpha,\kappa}(t_0)e^{-i\epsilon_{\alpha,\kappa}mT}\Phi_{\alpha,\kappa}(x,t_0). \tag{7}$$

B. Evaluation of the time evolution operator

It is apparent that, once the FBMs $\Phi_{\alpha,\kappa}$ are known, any quantum state $\Psi(x,mT)$ can be propagated stroboscopically according to Eq. (7). In the following we explain how the FBMs can be obtained numerically in an efficient way. The general idea is to make use of the fact that as mentioned above the FBMs are eigenstates of the one-period time evolution operator $U(T+t_0,t_0)$. Accordingly, once the matrix representation of this operator is calculated in some basis it can be diagonalized and one obtains both the FBMs $\Phi_{\alpha,\kappa}(x,t_0)$ and the corresponding QEs $\epsilon_{\alpha,\kappa}$.

1. The underlying Hilbert space

The first step towards the calculation of the matrix representation of the evolution operator, and with this of the FBMs, is to specify the Hilbert space $\mathcal{H}$ in which the solutions of the TDSE [Eq. (1)] can be represented. It was argued in [39] that $\mathcal{H}$ can be composed as a product space of the Hilbert space of square integrable functions $\mathcal{R}$ and of the Hilbert space of time-periodic functions $\mathcal{T}$.

In the following we define appropriate bases for $\mathcal{R}$, $\mathcal{T}$, and finally for $\mathcal{H}$. The states that we want to represent in $\mathcal{H}$, namely, the FBMs, have to obey Bloch's theorem. This imposes the condition that of the square integrable functions constituting the Hilbert space $\mathcal{R}$ we are interested only in the ones obeying $\Psi(x+n_pL) = e^{i\kappa n_pL}\Psi(x)$. We can take this into account by choosing quasimomentum-dependent basis vectors $\langle x|\mu_\kappa\rangle = \frac{1}{n_pL}e^{i[2\pi\mu/(Ln_p)+\kappa]x}$ for $\mu \in \mathbb{Z}$, which are in accordance with the Bloch theorem since $|\mu_\kappa\rangle = e^{i\kappa x}|\mu\rangle$ where $\langle x|\mu\rangle = \langle x+n_pL|\mu\rangle$. Hence, once the time evolution operator is obtained in this basis and the FBMs are calculated as its eigenvectors, they will automatically satisfy Bloch's theorem because the basis in which they are expanded does. The inner product in $\mathcal{R}$ can be defined as $\langle f|g\rangle = \int_{-\infty}^{\infty} dx f^*(x)g(x)$ for $|f\rangle, |g\rangle \in \mathcal{R}$. For the Hilbert space of time-periodic functions $\mathcal{T}$ the inner product is given by $\langle a|b\rangle = \frac{1}{T}\int dt\, a^*(t)b(t)$ for $|a\rangle, |b\rangle \in \mathcal{T}$ and the Fourier vectors $\langle t|n\rangle = e^{in\omega t}$ with $n \in \mathbb{Z}$ are a natural choice for the basis vectors.

As mentioned earlier, the entire solution space $\mathcal{H}$ of Eq. (1) can be constructed as the product space, $\mathcal{H} = \mathcal{R}\otimes\mathcal{T}$. Thus, a possible choice of basis vectors for $\mathcal{H}$ is given by the product basis $|\mu_\kappa\rangle \otimes |n\rangle \equiv |\mu_\kappa,n\rangle\rangle$ and the scalar product associated with $\mathcal{H}$ is

$$\langle\langle\Psi|\Psi'\rangle\rangle = \frac{1}{T}\int_0^T dt \int_{-\infty}^{+\infty} dx \Psi^*(x,t)\Psi'(x,t). \tag{8}$$

2. The time evolution operator

After we have specified the solution space of the TDSE we are ready to calculate its solutions, or more precisely its FBMs. As mentioned before, this can be done by finding the eigenvectors of the one-period time evolution operator $U(T+t_0,t_0)$.

It was shown in [36] that the time evolution operator represented in our basis of $\mathcal{R}$ can be calculated for zero quasimomentum as

$$U_{\mu\nu}(t,t_0) \equiv \langle\mu|\,U(t,t_0)\,|\nu\rangle = \sum_{n=-\infty}^{+\infty} \langle\langle\mu n|\,e^{-iH_f(t-t_0)}\,|\nu 0\rangle\rangle e^{in\omega t}, \tag{9}$$

where the Floquet operator $H_f(x,t) = H(x,t) - i\frac{\partial}{\partial t}$ was introduced. Because in this work the authors were interested in the time evolution of a single atom in a spatially homogeneous oscillating magnetic field, there was no need for the introduction of a nonzero quasimomentum. We, however, are interested in the action of a spatially periodic inhomogeneous potential and are therefore entitled to consider the case $\kappa \neq 0$ as well. In order to do this, we exploit the fact that states of different quasimomenta are of course not mixed through the action of the Hamiltonian. Thus the matrix representation of the time evolution operator $U_{\mu\nu}(t,t_0)$ can be thought of as being a block matrix, where every block acts only on states with a certain quasimomentum κ. For each of these blocks we introduce the notation $U^\kappa_{\mu\nu}(t,t_0)$. Equation (9) can be adjusted easily, by replacing the mere plane wave basis $|\mu\rangle$ with the κ-dependent basis vectors $|\mu_\kappa\rangle$ introduced in Sec. III B 1. Thus we obtain for the evolution operator for now arbitrary quasimomentum:

$$U^\kappa_{\mu\nu}(t,t_0) \equiv \langle\mu_\kappa|\,U(t,t_0)\,|\nu_\kappa\rangle = \sum_{n=-\infty}^{+\infty} \langle\langle\mu_\kappa n|\,e^{-iH_f(t-t_0)}\,|\nu_\kappa 0\rangle\rangle e^{in\omega t}, \tag{10}$$

which for $t = t_0 + T$ is the desired expression for the matrix elements of the time evolution operator over one driving

period. In the following we show how Eq. (10) can be evaluated numerically. To begin with, we divide the interval (t_0, t_0+T) into N small intervals of length Δt, thus allowing for a truncation of the exponential series for sufficiently small Δt. Hence, the quantity of interest becomes the evolution operator over the jth short time span Δt: $U^{\kappa,j}_{\mu\nu} = U^{\kappa}_{\mu\nu}[t_0 + j\Delta t, t_0 + (j-1)\Delta t]$ for $j = 1,\ldots,N$, while the full operator can be obtained as the product of all $U^{\kappa,j}_{\mu\nu}$ afterwards (we omit the matrix indices μ and ν for the sake of clarity):

$$U^{\kappa}(t_0+T,t_0) = U^{\kappa,N}(t_0)\cdots U^{\kappa,1}(t_0) = \prod_{j=1}^{N} U^{\kappa,j}(t_0). \tag{11}$$

From Eq. (10) we get

$$U^{\kappa,j}_{\mu\nu} = \lim_{p_{\max}\to\infty} \sum_{n=-\infty}^{+\infty} e^{in\omega j\Delta t} \sum_{p=0}^{p=p_{\max}} \frac{1}{p!}(-i\Delta t)^p \times \langle\!\langle \mu_\kappa n|\, H_f^p(x,t-t_0)\,|\nu_\kappa 0\rangle\!\rangle, \tag{12}$$

where in a numerical calculation $p_{\max}$ has to be sufficiently large to ensure convergence and $\langle\!\langle \mu_\kappa n|\, H_f^p(x,t)\,|\nu_\kappa 0\rangle\!\rangle$ are the matrix elements of the pth power of the Floquet operator $H_f(x,t)$. In [36] it was shown how these can be calculated recursively for $\kappa = 0$. For nonzero quasimomentum we obtain (see Appendix A)

$$\langle\!\langle \mu_\kappa n|\, H_f^p\,|\nu_\kappa 0\rangle\!\rangle \approx \sum_{n'=-n_{\max}}^{+n_{\max}} \sum_{\mu'=-\mu_{\max}}^{+\mu_{\max}} \left(H^{\kappa\,(n-n')}_{\mu\mu'} + n\omega\delta_{\mu\mu'}\delta_{nn'}\right) \times \langle\!\langle \mu'_\kappa n'|\, H_f^{(p-1)}\,|\nu_\kappa 0\rangle\!\rangle. \tag{13}$$

Thereby, $n_{\max}$ and $\mu_{\max}$ have to be sufficiently large to ensure convergence and $H^{\kappa\,(n-m)}_{\mu\nu}$ is the matrix element of the $(n-m)$th Fourier coefficient of $H(x,t)$ represented in the basis of $\mathcal{R}$, i.e.,

$$H^{\kappa\,(n-m)}_{\mu\nu} = \langle\mu_\kappa|\, H^{(n-m)}(x)\,|\nu_\kappa\rangle = \frac{1}{T}\int_0^T dt\, \langle\mu_\kappa|\, e^{-i\omega t(n-m)} H(x,t)\,|\nu_\kappa\rangle\,. \tag{14}$$

It is straightforward to see that the Fourier components of the Hamiltonian are

$$H^{\kappa,(n)}_{\mu\nu} = \frac{1}{2}\left(\frac{2\pi}{n_p L}\mu + \kappa\right)^2 \delta_{\mu\nu}\delta_{n0} + V^{(n)}_{\mu\nu} \tag{15}$$

with $V^{(n)}_{\mu\nu} = \langle\mu_\kappa|\, V^{(n)}(x)\,|\nu_\kappa\rangle$, where the κ dependence can be omitted since the potential is a function solely of the position operator and not of its derivatives, and therefore $V^{\kappa,(n)}_{\mu\nu} = \langle\mu_\kappa|\, V^{(n)}(x)\,|\nu_\kappa\rangle = \langle\mu|\, e^{-i\kappa x} V^{(n)}(x) e^{i\kappa x}\,|\nu\rangle = \langle\mu|\, V^{(n)}(x)\,|\nu\rangle = V^{(n)}_{\mu\nu}$.

3. The potential energy

So far we have seen how the time evolution operator $U^{\kappa}_{\mu\nu}(T+t_0,t_0)$ for a given quasimomentum κ can be calculated by evaluating the matrix elements of the powers of the Floquet operator as given by Eq. (13), which in turn requires the calculation of the Fourier components of the Hamiltonian via Eq. (15). The remaining task is to compute the Fourier components of the potential $V^{(n)}(x)$, or more precisely their matrix representations in $\mathcal{R}$: $V^{(n)}_{\mu\nu}$. Note that the formalism described so far does not distinguish between uniform and spatiotemporal driving. However, this becomes relevant for the Fourier decomposition of the potential $V^{(n)}(x)$ as we shall see in the following.

Let us start by considering the potential of a single oscillating barrier which will be denoted by $V_{\mathrm{SB}}(x,t)$ in the following. Performing a Fourier transformation yields $V_{\mathrm{SB}}(x,t) = \sum_{n=-\infty}^{+\infty} V^{(n)}_{\mathrm{SB}}(x) e^{in\omega t}$ with $V^{(n)}_{\mathrm{SB}}(x) \equiv \frac{1}{T}\int_0^T V_{\mathrm{SB}}(x,t) e^{in\omega t}$. If we now include a nonzero initial time t_0 as well as a possible phase of the barrier motion of δ [cf. Eq. (3)], we get via the transformation $t \to t + t_0 + \frac{\delta}{\omega}$

$$V_{\mathrm{SB}}(x,t) = \sum_{n=-\infty}^{+\infty} V^{(n)}_{\mathrm{SB}}(x) e^{in[\omega(t+t_0)+\delta]}. \tag{16}$$

Apparently, the phase shift δ of a barrier leads to a complex phase factor of $e^{in\delta}$ of the corresponding Fourier coefficient. For n_p barriers each with a different phase δ_s this generalizes to

$$V^{(n)}(x) = \sum_{s=1}^{n_p} V^{(n)}_{\mathrm{SB}}(x - x_{0,s}) e^{in(\omega t_0+\delta_s)}, \tag{17}$$

with $x_{0,s} = sL$ being the equilibrium position of the sth barrier. For the desired matrix representation of this Fourier mode $V^{(n)}_{\mu\nu}$ this yields (see Appendix B)

$$V^{(n)}_{\mu\nu} = \sum_{s=1}^{n_p} V^{(n)}_{\mathrm{SB},\,\mu\nu} e^{i[n(\omega t_0+\delta_s)+(2\pi/Ln_p)(\mu-\nu)x_{0,s}]}, \tag{18}$$

where $V^{(n)}_{\mathrm{SB},\,\mu\nu} = \langle\mu|\, V^{(n)}_{\mathrm{SB}}(x)\,|\nu\rangle$ is the nth Fourier component of a single oscillating barrier represented in our basis of $\mathcal{R}$.

At this point we have all the ingredients to make use of Eq. (12) in order to determine the one-period time evolution operator and thus the FBMs, the QEs, and finally the stroboscopic time evolution of arbitrary initial states via Eq. (7).

C. Computation for different initial times

The final remark of this section is on the role of the initial time within the described formalism. Due to the linearity of the Schrödinger equation, the asymptotic behavior of an observable in a time-dependent system depends, in general, on the initial time t_0. For example, in the context of ratchet physics it was shown that the asymptotic transport velocity of an initial state depends crucially on t_0 (see [6] and also Sec. VI). Thus, in numerical simulations the time propagation typically has to be performed for many different initial times in order to capture the full physical behavior. The straightforward way to include different initial times in the formalism as described above is to simply plug in the potential $V(x,t+t_0)$ into the calculation of the Fourier components of the Hamiltonian [via Eq. (15)]. The downside of this approach is that the entire formalism to calculate $U(T+t_0,t_0)$ has to be carried out for each considered value of t_0, which can be quite time consuming. Fortunately, there is a much faster way. Within the presented formalism we have calculated the time evolution operator over an entire driving period as the product of N operators $U^{\kappa,j}(t_0)$ where

each of the $U^{\kappa,j}(t_0)$ propagates over the small time step Δt [see Eq. (11)]. The idea is now to calculate the N operators $U^{\kappa,j}(t_0)$ for some value of the initial time, say for $t_0 = 0$. The desired operator $U(T + t_0, t_0)$ for arbitrary t_0 can be obtained simply as the product of all the $U^{\kappa,j}(t_0 = 0)$, where the dependence on t_0 is now captured in the ordering of the operators. More precisely, Eq. (11) can be rewritten for $0 \leqslant t_0 \leqslant T$ as

$$U^{\kappa}(t_0 + T, t_0) = (U^{\kappa,j_0-1} \cdots U^{\kappa,1})(U^{\kappa,N} \cdots U^{\kappa,j_0}) = \prod_{j=1}^{j_0-1} U^{\kappa,j}(t_0 = 0) \prod_{j=j_0}^{N} U^{\kappa,j}(t_0 = 0) \quad (19)$$

with $j_0 = \lceil (N/T)t_0 \rceil$ where $\lceil x \rceil$ denotes the smallest integer number larger than x. The obvious advantage is that the $U^{j,\kappa}(t_0)$ have to be calculated only for one initial time. Afterwards, the time evolution operators for arbitrary initial times can be calculated easily by means of matrix multiplication. For the calculation of the FBMs in the setup of the spatiotemporally driven lattice, the speedup of this procedure to include the dependence of the initial time—as compared to the previously mentioned straightforward way—proved to be significant and amounted to up to one order of magnitude.

IV. SYMMETRY ANALYSIS

It goes without saying that classifying the symmetries of a physical system is often helpful in order to understand the phenomena occurring in it. In the context of quantum ratchets, for example, how the symmetries of the Floquet operator affect the possibility of directed particle motion has been extensively studied [12,17]. Within this section we present the relevant symmetries of the Hamiltonian and deduce their consequences for the time evolution operator as well as for the FBMs. As it turns out, the unitary symmetries corresponding to parity and spatial shifts as well as the antiunitary time-reversal symmetry will be of major importance. Hence, our analysis will start with general remarks on time-reversal and parity symmetry which are commonly studied in the context of uniformly driven one-dimensional (1D) lattices [17]. Afterwards, we investigate the impact of the spatiotemporal driving.

A. Time-reversal symmetry

The Hamiltonian is symmetric under time reversal if $H(x,t) = H(x, -t + \tau)$ for some appropriate time shift τ, which we will assume to be zero in the following. Let us start with investigating the consequences of time-reversal symmetry for the time evolution operator $U(t,t_0)$. For the simpler case of zero quasimomentum it was shown in [40] that the matrix elements of $U(T,0)$ in the plane wave basis as used in this work obey

$$U_{-\nu-\mu}(T/2,0) = U_{\mu\nu}(T,T/2), \quad U_{-\nu-\mu}(T,0) = U_{\mu\nu}(T,0). \quad (20)$$

Of particular interest is the last named symmetry because it concerns the time evolution operator over an entire driving period, which is the one used to determine the FBMs [see Eq. (5)]. By employing ideas from Sec. III one can readily generalize this symmetry to nonzero values of the quasimomentum κ: At the heart of the calculation of the matrix elements of the time evolution operator as given by Eq. (10) is the calculation of the Fourier components of the Hamiltonian as given by Eq. (15). Note that the quasimomentum κ enters only in the diagonal term which is proportional to $(\frac{2\pi}{n_p L}\mu + \kappa)^2 \delta_{\mu\nu}$. Apparently, this term is invariant under $\mu \to -\nu$ if and only if we set $\kappa \to -\kappa$ simultaneously. Thus the symmetry generalizes for arbitrary quasimomentum κ to

$$U^{-\kappa}_{-\nu-\mu}(T,0) = U^{\kappa}_{\mu\nu}(T,0). \quad (21)$$

In fact we find strong evidence that both symmetries as stated in Eq. (20) are special cases of the more general symmetry which holds here:

$$U^{-\kappa}_{-\nu-\mu}(t_2,t_1) = U^{\kappa}_{\mu\nu}(T - t_1, T - t_2) \quad (22)$$

with $0 < t_1 < t_2 < T$. In Appendix C we provide a rigorous proof up to first order in the expansion of the time evolution operator, i.e., for $p_{\max} = 1$ in Eq. (12). Beyond first order, we have strong numerical evidence for the validity of Eq. (22).

Finally, we consider the consequence of a time-reversal symmetry of the Hamiltonian on the FBMs. It was argued in [17] that these must obey

$$\Phi_{\alpha,\kappa}(x,t) = \sigma_\alpha \Phi^*_{\alpha,-\kappa}(x, T - t), \quad \sigma_\alpha = \pm 1. \quad (23)$$

For the representation as chosen in this work, this yields for the components of the FBMs

$$\langle \mu | \Phi_{\alpha,\kappa}(x,t) \rangle \equiv \Phi^{\mu}_{\alpha,\kappa}(t) = \sigma_\alpha \left[\Phi^{-\mu}_{\alpha,-\kappa}(T - t) \right]^*. \quad (24)$$

B. Parity symmetry

The Hamiltonian is said to be invariant under parity symmetry if $H(x,t) = H(-x + \chi, t + T/2)$ for some appropriate spatial shift χ which we can assume without loss of generality to be zero. As argued in [40] parity symmetry yields for the time evolution operator

$$U^{\kappa}_{\mu\nu}(T,0) = \sum_{\theta} U^{\kappa}_{-\mu-\theta}(T/2,0) U^{\kappa}_{\theta\nu}(T/2,0). \quad (25)$$

This relation can be of particular use since it allows us to halve the computational effort. Furthermore, this symmetry of the time evolution operator leads to a symmetry of the FBMs [17]:

$$\Phi_{\alpha,\kappa}(x,t) = \sigma_\alpha \Phi_{\alpha,-\kappa}(-x, t + T/2), \quad \sigma_\alpha = \pm 1. \quad (26)$$

In analogy to the time-reversal symmetry [see Eq. (24)] this yields for the components of the FBMs in the representation introduced in Sec. III

$$\Phi^{\mu}_{\alpha,\kappa}(t) = \sigma_\alpha \Phi^{-\mu}_{\alpha,-\kappa}(t + T/2). \quad (27)$$

C. Parity and time-reversal symmetry

Apparently, there is the possibility for a Hamiltonian to be symmetric under both parity and time-reversal symmetry. In this case it obeys $H(x,t) = H(-x, -t + \tau)$. The components of the Floquet modes have to fulfill both Eq. (24) and Eq.(27). Hence we get

$$\Phi^{\mu}_{\alpha,\kappa}(T - t) = \sigma_\alpha \left[\Phi^{\mu}_{\alpha,\kappa}(t + T/2) \right]^*. \quad (28)$$

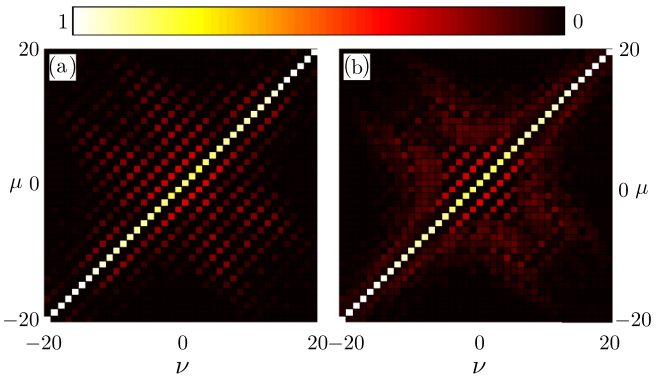

FIG. 2. (Color online) Absolute value of matrix elements $U_{\mu\nu}(T,0)$ of the time evolution operator for $\kappa = 0$. The phases δ_s of the three barriers within one unit cell are (0,0,0) in (a) and $(0,\pi,0)$ in (b). The remaining parameters are $L = 10$, $V_0 = 1.0$, $\omega = 1.0$, $A = 1.0$, and $\Delta = 0.5$.

D. Shift symmetry

Finally we turn our focus to the impact of spatiotemporal driving and investigate its consequences for the time evolution operator as well as for the FBMs. Let us as an introductory example consider a lattice with a unit cell which contains three barriers, i.e., we have $n_p = 3$. We choose for the three different initial phases δ_s for $s = 1,2,3$ in the driving law [see Eq. (3)] ($\delta_1 = 0$, δ_2, $\delta_3 = 0$) with $\delta_2 \in [0,2\pi)$. Hence, we obtain a driven lattice where the central barrier of each unit cell is potentially out of phase compared to its two neighboring barriers. In the following we try to deduce properties of the overall structure of the time evolution operator for such a setup. In doing so, we will show that this "partial shift symmetry breaking" induced by the complex nature of the unit cell in a spatiotemporally driven lattice has profound consequences both on the time evolution operator and on the FBMs.

To get some insight we calculate numerically the matrix elements of the time evolution operator $U_{\mu\nu}(T,0)$ for zero quasimomentum and for $t_0 = 0$. We do this for the case of a nonzero phase shift of the central barrier of $\delta_2 = \pi$ and compare the results to the uniformly driven lattice with $\delta_2 = 0$. The absolute values of the obtained $U_{\mu\nu}(T,0)$ are shown in Fig. 2. The most intriguing feature is that in both cases we observe a stripelike structure for the nonzero elements. In particular, for the uniformly driven case [Fig. 2(a)] we see that for a fixed value of μ, only every third value of ν corresponds to a nonzero matrix element, and vice versa. For the spatiotemporally driven lattice [Fig. 2(b)] this behavior persists for elements close to the main diagonal but becomes less pronounced further away from it, i.e., for larger values of $|\mu - \nu|$.

In order to understand the overall structure of the two time evolution operators shown, we consider their different symmetries under spatial shifts. Obviously both Hamiltonians obey $H(x,t) = H(x + n_pL,t)$ because by construction the length of the unit cell was chosen to be n_pL. However, in the uniformly driven case, the Hamiltonian additionally obeys $H(x,t) = H(x + L,t)$, and consequently the time evolution operator $U_{\mu\nu}(T,0)$ should commute with the operator $S^L = e^{-iL\hat{p}} = e^{-L\partial/\partial x}$ performing a spatial shift of L. This is because the FBMs form a complete set and are eigenstates of both $U_{\mu\nu}(T,0)$ and S^L. For arbitrary quasimomentum κ the matrix representation of the shift operator S^L becomes

$$S^{\kappa,L}_{\mu\nu} = \langle \mu_\kappa | \, S^L \, | \nu_\kappa \rangle = e^{-i[(2\pi/n_pL)\mu+\kappa]L}\delta_{\mu\nu}. \tag{29}$$

Thus the requirement of commutation with $S^{\kappa,L}_{\mu\nu}$ yields for the matrix elements $U_{\mu\nu}(T,0)$ (we omit the argument for the sake of clarity)

$$S^{\kappa,L}_{\mu\beta}U_{\beta\nu} - U_{\mu\gamma}S^{\kappa,L}_{\gamma\nu} = (e^{-i(2\pi/n_p)\mu} - e^{-i(2\pi/n_p)\nu})U_{\mu\nu} \stackrel{!}{=} 0. \tag{30}$$

Apparently, this requires that either $U_{\mu\nu}(T,0) = 0$ or $\mu - \nu = n_pz$ for $z \in \mathbb{Z}$ and explains the stripelike structure of the time evolution operator as observed in Fig. 2(a). Arguments along a very similar line lead to a restriction on the components of the FBMs $\Phi^\mu_{\alpha,\kappa}(t)$. Due to the Bloch theorem the FBMs must be eigenstates of S^L and thus

$$S^{\kappa,L}_{\mu\nu}\Phi^\nu_{\alpha,\kappa}(t) = e^{-i(2\pi/n_p)\mu}e^{-i\kappa L}\Phi^\mu_{\alpha,\kappa}(t) \stackrel{!}{=} \lambda_\alpha\Phi^\mu_{\alpha,\kappa}(t) \tag{31}$$

for some complex eigenvalue λ_α. This requires that the prefactor $e^{-i(2\pi/n_p)\mu}$ must be independent of μ which is true only if all the nonzero components of the FBM $\Phi^\mu_{\alpha,\kappa}(t)$ can be labeled by $\mu = n_pz + q$ for $z \in \mathbb{Z}$ and $q = 0,1,\ldots,n_p - 1$. The corresponding n_p different eigenvalues are $\lambda_{\alpha,q} = e^{-i[(2\pi/n_p)q+L\kappa]}$.

Although the reported restrictions on the matrix elements $U_{\mu\nu}$ as well as on the FBMs were derived for the uniformly driven lattice with $\delta_2 = 0$, we see clearly that, for the case of the evolution operator, this structure survives to some degree even for the largest possible phase shift of $\delta_2 = \pi$ [cf. Fig. 2(b)]. For decreasing δ_2 we observe that the uniformly driven case is approached more and more closely.

E. Husimi representations for uniform and spatiotemporal driving

We conclude the section on the symmetry analysis by analyzing the consequences of the discussed symmetries on Husimi representations, which are a very commonly used tool to obtain a coarse-grained visualization of a quantum state [41]. The Husimi representation of a quantum state is defined by the square of the absolute value of its overlap with a coherent state $|\rho(x,p)\rangle$ centered around position x, with momentum p, and with width σ [41]. Such a coherent state can be expressed as $\langle\tilde{x}|\rho(x,p)\rangle = (\pi\sigma^2)^{-1/4}e^{-(x-\tilde{x})^2/2\sigma^2+ip\tilde{x}}$. For a FBM $\Phi_\kappa(x,t)$ with quasimomentum κ we can calculate the Husimi distribution $Q_\kappa(x,p,t)$ as

$$Q_\kappa(x,p,t) = \frac{1}{2\pi}|\langle\rho(x,p)|\Phi_\kappa\rangle|^2 = \frac{(\pi\sigma^2)^{-1/4}}{2\pi}\left|\int d\tilde{x}\; e^{-(x-\tilde{x})^2/2\sigma^2+ip\tilde{x}}\Phi_\kappa(\tilde{x},t)\right|^2$$
$$= \sqrt{2\pi}\left|\sum_\mu \Phi^\mu_\kappa(t)\; e^{-(\sigma^2/2)[(2\pi/n_pL)\mu+\kappa-p]^2+i[(2\pi/n_pL)\mu+\kappa-p]x}\right|^2, \tag{32}$$

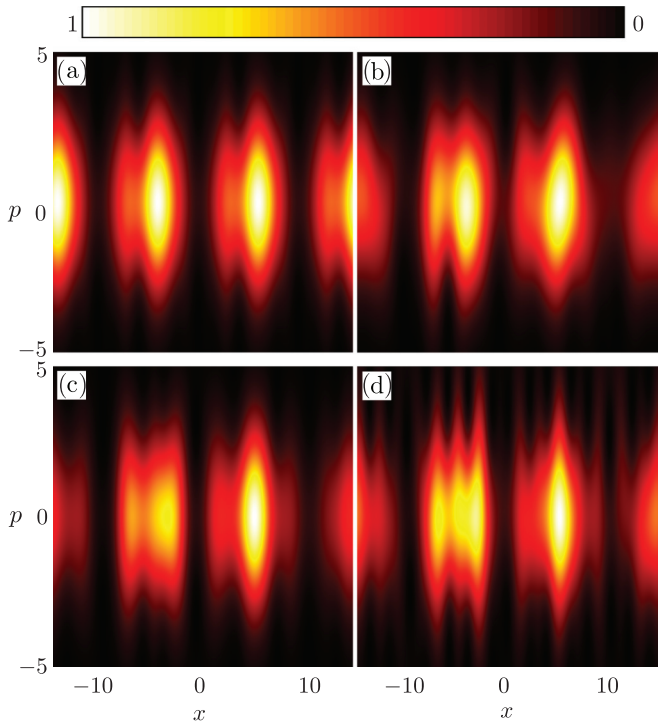

FIG. 3. (Color online) Husimi distributions in arbitrary units for $\sigma = 0.5$ of a FBM at zero quasimomentum in a lattice with $n_p = 3$ for four different settings of the barrier phases $(\delta_1,\delta_2,\delta_3)$: (a) $(0,0,0)$, (b) $(0,\pi/2,0)$, (c) $(0,\pi,0)$, and (d) $(0,\pi,\pi/4)$. The barrier equilibrium positions are at $x_1 = -10$, $x_2 = 0$, and $x_3 = 10$. The remaining parameters are as in Fig. 2.

where we have plugged in the expansion of the FBM $\Phi_\kappa(x,t)$ in terms of our basis of $\mathcal{R}$: $\Phi_\kappa(x,t) = \sum_\mu \Phi_\kappa^\mu(t) e^{-i[(2\pi/n_p L)\mu+\kappa]x}$. To get some insight, let us consider the Husimi representation of one specific FBM. This mode, denoted as $\Phi_G(x,t)$, has zero quasimomentum and is characterized as the FBM with the largest overlap with a spatially uniform state. It is of particular importance since it usually also has the largest overlap with a quantum particle which is initially distributed over many lattice sites—a situation that is commonly considered both in theory and in experiments [12]. The Husimi distributions $Q(x,p,t)$ of $\Phi_G(x,t)$ for $t = 0$ are shown for different setups each containing three barriers per unit cell ($n_p = 3$) but with different settings of the barrier phases $(\delta_1,\delta_2,\delta_3)$ [cf. Eq. (3)] in Fig. 3. For the uniformly driven lattice [Fig. 3(a)] we observe that the Husimi representation is invariant under a spatial shift of one barrier distance L, i.e., $Q(x,p,0) = Q(x+L,p,0)$. Apparently, this shift symmetry is broken for setups with nonzero barrier phases [Figs. 3(b), 3(c), and 3(d)]. Additionally, for the setups with $(0,0,0)$ and $(0,\pi,0)$ the Husimi distribution is symmetric with respect to an inversion of momentum, i.e., we observe $Q(x,p,0) = Q(x,-p,0)$. In the following we argue how these symmetries of the Husimi representations can be deduced from the corresponding symmetry analysis.

Let us start with the observed shift symmetry $Q(x,p,0) = Q(x+L,p,0)$. In fact, it follows directly from the shift symmetry of the FBM which obeys $\Phi_G(x,t) = \Phi_G(x+L,t)$ (cf. Sec. IV D) that the shift symmetry of the Husimi distribution indeed holds for all times. Likewise, the observed symmetry of $Q(x,p,0) = Q(x,-p,0)$ can be understood conveniently with the help of the above symmetry analysis. By virtue of Eq. (24) we know that $\Phi_G^\mu(0) = [\Phi_G^{-\mu}(0)]^*$ which can be shown easily to imply $Q(x,p,0) = Q(x,-p,0)$. More generally, one can show from Eq. (32) that the restrictions on the FBMs in the presence of time-reversal symmetry [see Eq. (24)] yield for the Husimi representation

$$Q^\kappa(x,p,t) = Q^{-\kappa}(x,-p,T-t). \tag{33}$$

Analogously, the presence of parity symmetry, where the components of the FBMs obey Eq. (27), implies for the Husimi representation

$$Q^\kappa(x,p,t) = Q^{-\kappa}(-x,-p,t+T/2). \tag{34}$$

Note that even though we used a particular representation of the FBMs in order to derive the two latter relations for the Husimi distribution, these relations themselves must of course hold for every other representation too. Thus Eqs. (33) and (34) are general results for FBMs in 1D driven lattices with time-reversal or parity symmetry.

Because the Hamiltonians underlying Figs. 3(a) and 3(c) with phases $(0,0,0)$ and $(0,\pi,0)$ respect both time-reversal and parity symmetry, the Husimi distributions obey Eqs. (33) and (34). The setup with $(0,\pi/2,0)$ as used in Fig. 3(b) inherits only parity symmetry, i.e., the associated $Q(x,p,t)$ obeys only Eq. (34). Finally, for $(0,\pi,\pi/4)$ no symmetry remains.

V. THE FLOQUET SPECTRUM

The quasienergies $\epsilon_{\alpha,\kappa}$ of the FBMs $\Phi_{\alpha,\kappa}(x,t)$ evaluated as functions of the quasimomentum κ constitute the quasienergy or Floquet spectrum of a periodically driven system. In the following we investigate the impact of the symmetries as introduced in Sec, IV on the Floquet spectrum. This question has been the subject of comprehensive research in the case of uniform driving (see, e.g., [11,12,17,18]), and we are going to sum up the most important results. However, our main interest is in the impact of the partially broken shift symmetry induced by the spatiotemporal driving. As before we consider as an exemplary setup a lattice with a unit cell containing three barriers with phases $(\delta_1,\delta_2,\delta_3)$.

A. Impact of parity and/or time-reversal symmetry

An extract of the Floquet spectrum for a phase configuration of $(\delta_1 = 0, \delta_2 = \frac{2\pi}{3}, \delta_3 = 0)$ is shown in Fig. 4(a). In this case the Hamiltonian is invariant under parity symmetry as introduced in Sec. IV and we observe that $\epsilon_{\alpha,\kappa} = \epsilon_{\alpha,-\kappa}$, i.e., the spectrum is symmetric with respect to $\kappa = 0$. In fact it was argued in [17] that the invariance of the Hamiltonian under either parity or time-reversal symmetry generally yields a spectrum which is symmetric with respect to $\kappa = 0$. In accordance with this, it is shown how a breaking of these symmetries by setting a second barrier phase, in this case δ_3, to a nonzero value leads to a desymmetrization of the spectrum. Note that for such a configuration where we fix two barrier phases to $\delta_1 = 0$ and have arbitrary δ_2, parity symmetry is always present for $\delta_3 = 0$. Thus by changing the value of the phase of the third barrier δ_3 from zero, one can very reliably tune the asymmetry of the spectrum.

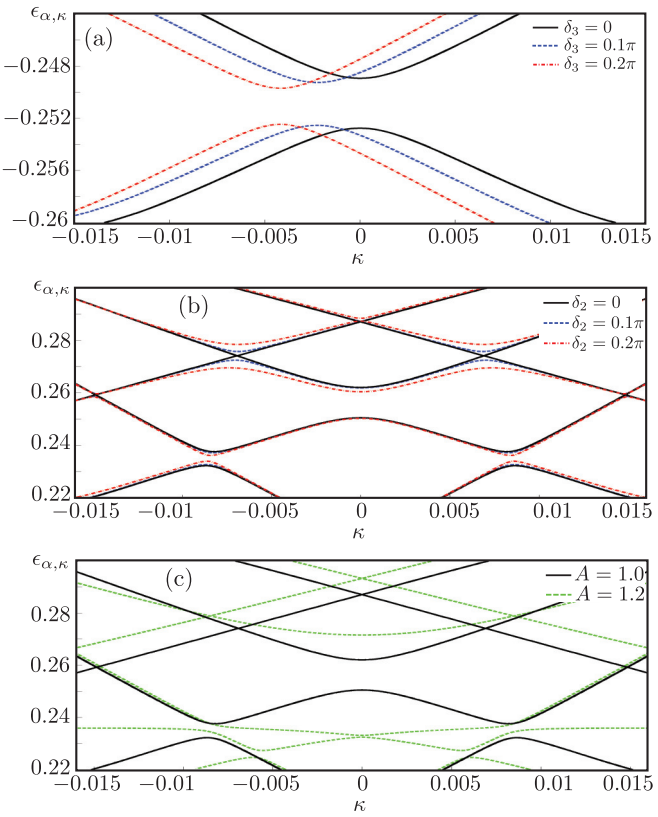

FIG. 4. (Color online) Extracts of the Floquet spectra for different setups containing three barriers per unit cell. The three phases of the barrier driving laws are (a) $(0,2\pi/3,\delta_3)$, (b) $(0,\delta_2,0)$, and (c) (0,0,0). In (c) the spectra for two different global driving amplitudes are shown. The remaining parameters are as in Fig. 2.

B. The role of shift symmetry and transitions from exact to avoided crossings

In the following we show how the deviation from a uniform driving towards a spatiotemporal driving affects the Floquet spectrum in a unique way. As a model system we consider a phase configuration of the barriers in a unit cell of $(0,\delta_2,0)$, where as in Sec. IV D the shift symmetry is said to be "partially broken" for $\delta_2 \neq 0$. Representative extracts of the spectrum for uniform driving ($\delta_2 = 0$) as well as for a spatiotemporal driving ($\delta_2 \neq 0$) are shown in Fig. 4(b). The most notable effect is that the crossings which are exact for the uniform driving are cast into avoided crossings in the case of the spatiotemporal driving. At the same time the crossings which are avoided for uniform driving remain avoided crossings for $\delta_2 \neq 0$. Further, we see that at least to a certain degree one can control the width of the avoided crossing by tuning the phase of the central barrier δ_2. This is best seen for the two crossings at $\epsilon \approx 0.275$ where the widths can be seen to increase for increasing δ_2. At this point it is worth mentioning that the widths of avoided crossings in Floquet spectra are crucial for many nonequilibrium phenomena reported in driven lattice setups, such as Landau-Zener transitions [18], the diffusion properties of a wavepacket [35], or the occurrence of an absolute negative mobility [7]. Hence, the additional flexibility introduced by the site-dependent driving should contribute to an increased controllability of the aforementioned effects.

For comparison we also show the spectrum of a uniformly driven lattice for two different driving amplitudes $A = 1.0$ and $A = 1.2$ in Fig. 4(c). Apparently, even though the spectrum is altered significantly by the increased driving amplitude, the nature of the crossings, i.e., exact or avoided, is not changed.

By means of the symmetry analysis carried out in Sec. IV D it is quite straightforward to understand why the variation in the barrier phase δ_2 leads to a transformation of the crossings from exact to avoided while the variation in the global driving amplitude A does not. The key observation lies within Eq. (31), stating that the FBMs must be eigenstates of the operator performing a spatial shift of the barrier distance L. As argued, the allowed eigenvalues for a FBM $\Phi_{\alpha,\kappa}(x,t)$ are then given by $\lambda_{\alpha,q} = e^{-i[(2\pi/n_p)q+L\kappa]}$ for $q = 0,1,\ldots,n_p - 1$. Thus the FBMs can be separated into n_p different symmetry classes, each characterized by one of the n_p different eigenvalues $\lambda_{\alpha,q}$. According to the noncrossing rule [42] states belonging to different symmetry classes are allowed to cross, while states within the same symmetry class cannot. For a nonzero value of δ_2 the shift symmetry $x \to x + L$ gets destroyed and Eq. (31) becomes invalid. Hence, the FBMs cannot be separated into different symmetry classes associated with the shift operator S^L and thus they are not allowed to cross anymore. At this point it is important to note that, even for a partially broken shift symmetry, the spectrum may still feature exact crossings due to the presence of different symmetry classes associated with parity or time-reversal symmetry.

VI. DIRECTED TRANSPORT

In this section, we study the possibility of an asymptotic particle current in the setup of a spatiotemporally driven lattice. The appearance of such currents in the absence of any mean forces has been studied intensively over the last two decades for uniformly driven lattices (see, for example, [1,9,17] and references therein). Similarly to the previous sections, we begin with some general considerations and investigate the spatiotemporally driven lattice in particular afterwards.

A. Asymptotic currents

Following [12] we define the asymptotic quantum current as the time-averaged expectation value of the momentum operator for some initial state $|\Psi_I(t_0)\rangle$:

$$J(t_0) = \lim_{t\to\infty} \frac{1}{t - t_0} \int_{t_0}^{t} d\tilde{t}\ \langle \Psi_I(\tilde{t})|\hat{p}|\Psi_I(\tilde{t})\rangle\,. \tag{35}$$

One of the perks of using Floquet theory in order to study the dynamics of a time-dependent system is that once the FBMs are known, the asymptotic current can be calculated very conveniently as [11,12]

$$J(t_0) = \int d\kappa \sum_{\alpha} v_{\alpha\kappa} |C_{\alpha\kappa}(t_0)|^2, \tag{36}$$

where $v_{\alpha\kappa}$ is the averaged momentum of the FBM $|\Phi_{\alpha\kappa}\rangle$ and $C_{\alpha\kappa}(t_0)$ is the overlap of the initial state with the FBM $|\Phi_{\alpha\kappa}\rangle$ at time $t = t_0$. For a commonly studied initial state of a Gaussian wave packet $\Psi_I(x,t_0) = (\pi\sigma^2)^{-1/4} e^{-x^2/2\sigma^2}$ these

two quantities can be calculated as

$$v_{\alpha\kappa} = \frac{1}{T}\int_0^T dt\, \langle \Phi_{\alpha\kappa}|\hat{p}|\Phi_{\alpha\kappa}\rangle$$
$$= \frac{1}{T}\sum_\mu \int_0^T dt \left(\frac{2\pi}{Ln_p}\mu + \kappa\right) \left|\Phi^\mu_{\alpha\kappa}(t)\right|^2,$$
$$C_{\alpha\kappa}(t_0) = \langle \Psi_I|\Phi_{\alpha\kappa}\rangle$$
$$= \frac{\sqrt{2\sigma}}{\pi^{-1/4}}\sum_\mu e^{-(\sigma^2/2L^2n_p^2)(n_pL\kappa+2\pi\mu)^2}\Phi^\mu_{\alpha\kappa}(t_0), \quad (37)$$

where as before the $\Phi^\mu_{\alpha\kappa}(t)$ are the components of the FBMs in our chosen basis, which can be calculated according to the numerical scheme presented in Sec. III.

B. Symmetries and directed transport

Now that we have seen how the asymptotic current $J(t_0)$ can be expressed through the components of the FBMs $\Phi^\mu_{\alpha\kappa}(t)$ we are able to analyze how the symmetries derived in Sec. IV for the $\Phi^\mu_{\alpha\kappa}(t_0)$ are carried over into symmetries of $J(t_0)$. For a time-reversal-symmetric Hamiltonian we saw that $\Phi^\mu_{\alpha,\kappa}(t) = \pm[\Phi^{-\mu}_{\alpha,-\kappa}(T-t)]^*$. From this and by virtue of Eq. (37) we readily calculate that $v_{\alpha\kappa} = -v_{\alpha-\kappa}$, which is in accordance with the arguments in [17]. For the overlap coefficients Eq. (37) yields $|C_{\alpha\kappa}(t)|^2 = |C_{\alpha-\kappa}(T-t)|^2$, which ultimately gives

$$J(t_0) = -J(T-t_0) \quad (38)$$

from Eq. (36). Analogously, the presence of parity symmetry induces $|C_{\alpha\kappa}(t)|^2 = |C_{\alpha-\kappa}(t+T/2)|^2$. For the asymptotic currents this results in

$$J(t_0) = -J(t_0+T/2). \quad (39)$$

Note that in the presence of either time-reversal or parity symmetry the asymptotic current averaged over the initial time vanishes, i.e., $\tilde{J} \equiv 1/T\int_0^T J(t)\,dt = 0$.

C. Transport in the spatiotemporally driven lattice

In the following we demonstrate transport phenomena in the spatiotemporally driven lattice. As an exemplary setup we again consider a lattice with three barriers in a unit cell, i.e., $n_p = 3$. The phases of the barriers are $(\delta_1,\delta_2,\delta_3)$ with $\delta_1 = 0$ and $\delta_2 = 2\pi/3$.

We calculate the asymptotic quantum current $J(t_0)$ numerically for different values of the third barrier phase δ_3 and for different initial times t_0. The results are shown in Fig. 5(a). For the case of $\delta_3 = 0$ the Hamiltonian possesses parity symmetry and thus according to the previous section the asymptotic current obeys $J(t_0) = -J(t_0+T/2)$. If δ_3 deviates from zero, parity symmetry is absent, which allows for a nonzero averaged current. Interestingly, for the small values of δ_3 shown, it seems that the curve $J(t_0)$ is merely shifted by some constant while the overall shape is approximately independent of δ_3. This also matches the observation concerning the variation of the Floquet spectrum for small deviations from a parity-symmetric setup [cf. Fig. 4(a)]. In this case, we observed that the spectrum approximately maintains its overall form, but the symmetry axis of the spectrum, which is at $\kappa = 0$ for $\delta_3 = 0$, is shifted to a nonzero κ for small nonzero δ_3. In order to understand how these two observations could be related, let us consider only the most populated Floquet mode for our initial state of a Gaussian wave packet, which for a parity-symmetric setup with $\delta_3 = 0$ has zero quasimomentum. As a crude approximation, one can argue that for a small deviation from $\delta_3 = 0$ this mode will remain almost unchanged but is shifted to a nonzero quasimomentum in the same way that the spectrum is. Hence, the mode picks up a momentum which is related to the shift of the spectrum and thus related to the value of δ_3. Furthermore, the spectrum is of course independent of the initial time and consequently the shift of the spectrum is the same for every t_0, which by virtue of the previous arguments would explain why the increase of $J(t_0)$ for increasing δ_3 was to a good approximation independent of t_0.

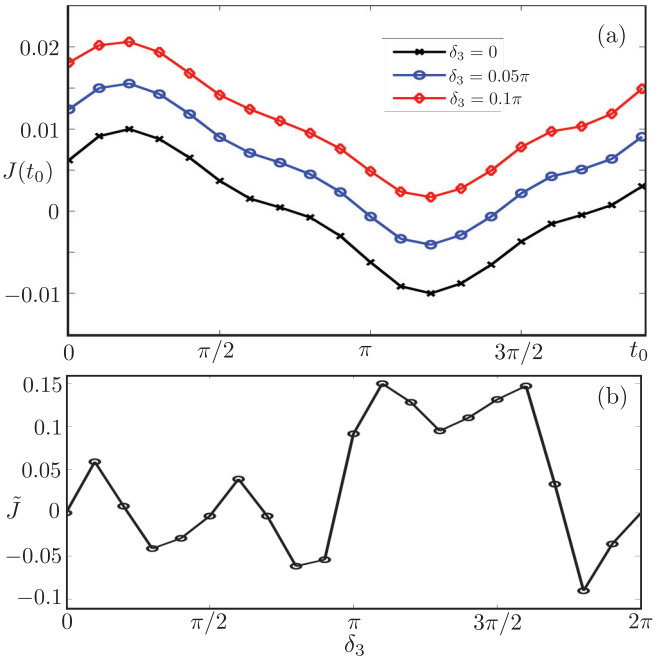

FIG. 5. (Color online) (a) Asymptotic quantum current $J(t_0)$ for three different configurations of the barrier phases $(0,2\pi/3,\delta_3)$. (b) Time-averaged quantum current as a function of the third barrier phase δ_3. The lines are guides for the eye. The remaining parameters are as in Fig. 2.

For larger values of the third barrier phase δ_3 the simple picture of a merely shifted spectrum is no longer applicable. The current averaged over the initial time is shown over the entire range of δ_3 in Fig. 5(b), revealing the more complex behavior at larger δ_3, such as several sign changes of the currents which cannot be explained easily be means of simple symmetry arguments. In fact it was shown in [12] that the asymptotic quantum current as a function of some system parameter generally features a highly nontrivial dependence.

VII. CONCLUSION AND OUTLOOK

We have investigated the setup of a quantum particle in a periodic lattice consisting of driven Gaussian barriers. Since we allowed for different driving laws which were spatially periodically repeated, we have been able to design

lattices with complex unit cells containing differently driven barriers. Within the framework of Floquet theory, we presented an efficient numerical scheme that provided us with the Floquet-Bloch modes for arbitrary quasimomentum. For the Floquet spectrum we found that the site-dependent driving has remarkable ramifications. A small deviation from a uniform, i.e., site-independent, driving was shown to cast exact into avoided crossings while the quasienergy bands away from the crossings remained approximately unaltered. The width of the corresponding avoided crossings could be manipulated by adjusting parameters of the driving law. Because the presence of exact and avoided crossings in the Floquet spectrum of driven lattice systems has been shown in the literature to be at the heart of many interesting phenomena, such as resonances in directed particle motion [12], the diffusion of a wave packet [35], the stimulation of Landau-Zener transitions via external forces [18], or even the possibility of an absolute negative mobility [7], this control over the crossing's widths as achieved in this work opens up a promising direction of interesting future research. We could explain the effect of a transition from a crossing to an avoided crossing as the result of a breaking of the translational symmetry over the distance apart of two adjacent barriers. Since this effect was shown to be symmetry induced it in no way depends on the fine-tuning of parameters and should be accessible in state-of-the-art cold atom experiments. Promising experimental techniques for the realization of the required breaking of translational invariance are subwavelength lattices where modulations below the laser's wavelength can be obtained [33]. Possible setups which should allow for the phase-modulated driving as studied in this work are provided by so-called painted potentials where full control over the motion of each potential barrier is achieved [34]. Here we showed that directed particle motion can be generated even in situations where each barrier on its own does not break the necessary symmetries. Over a certain regime the resulting currents were shown to be controllable by engineering the asymmetry of the Floquet spectrum through parameter variations of the site-dependent driving.

ACKNOWLEDGMENT

We thank H. Schanz for helpful discussions.

APPENDIX A: POWERS OF THE FLOQUET OPERATOR

The quantities of interest are the matrix elements of the powers of $H_f(x,t)$, i.e., we need to compute $\langle\langle \mu_\kappa n|\, H_f^p\, |\nu_\kappa m\rangle\rangle$. For $p=0$ one simply gets $\langle\langle \mu_\kappa n|\, \mathbf{1}\, |\nu_\kappa m\rangle\rangle = \delta_{\mu\nu}\delta_{nm}$ due to the orthonormality of the basis vectors. For $p=1$ we obtain

$$\begin{aligned}
&\langle\langle \mu_\kappa n|\, H_f(x,t)\, |\nu_\kappa m\rangle\rangle \\
&= \frac{1}{T}\int_0^T dt\, e^{-in\omega t}\, \langle \mu_\kappa|\left(H(x,t) - i\frac{\partial}{\partial t}\right)|\nu_\kappa\rangle\, e^{im\omega t} \\
&= \langle \mu_\kappa|\, H^{(n-m)}(x)\, |\nu_\kappa\rangle + \langle \mu_\kappa|\, m\omega\, |\nu_\kappa\rangle\, \delta_{\mu\nu} \\
&= H_{\mu\nu}^{\kappa\,(n-m)} + m\omega\delta_{mn}\delta_{\mu\nu}. \qquad \text{(A1)}
\end{aligned}$$

Matrix representations of higher powers of $H_f(x,t)$ can be calculated recursively:

$$\begin{aligned}
&\langle\langle \mu_\kappa n|\, H_f^p(x,t)\, |\nu_\kappa m\rangle\rangle \\
&= \langle\langle \mu_\kappa n|\, H_f(x,t) H_f^{p-1}(x,t)\, |\nu_\kappa m\rangle\rangle \\
&= \sum_{\mu' n'} \langle\langle \mu_\kappa n|\, H_f(x,t)\, |\mu'_\kappa n'\rangle\rangle\, \langle\langle \mu'_\kappa n'|\, H_f^{p-1}(x,t)\, |\nu_\kappa m\rangle\rangle \\
&= \sum_{\mu' n'} \left(H_{\mu\mu'}^{\kappa\,(n-n')} + n\omega\delta_{nn'}\delta_{\mu\mu'}\right)\langle\langle \mu'_\kappa n'|\, H_f^{p-1}(x,t)\, |\nu_\kappa m\rangle\rangle, \qquad \text{(A2)}
\end{aligned}$$

where we have used the completeness of the product basis as well as Eq. (A1).

APPENDIX B: FOURIER EXPANSION OF THE POTENTIAL

The Fourier coefficients of the potential $V^{(n)}(x)$ are to be represented in the basis of $\mathcal{R}$. Again we exploit the fact that we can omit the κ dependence for the operator of the potential energy, and the calculation becomes

$$\begin{aligned}
V_{\mu\nu}^{(n)} &= \langle \mu|\, V^{(n)}(x)\, |\nu\rangle \\
&= \frac{1}{L}\int_{-\infty}^{+\infty} dx\, V^{(n)}(x) e^{i(2\pi/Ln_P)(\nu-\mu)x} \\
&= \frac{1}{L}\int_{-\infty}^{+\infty} dx \sum_{s=1}^{n_p} V_{\mathrm{SB}}^{(n)}(x - x_{0,s}) e^{in(\omega t_0+\delta_s)} e^{i(2\pi/Ln_P)(\nu-\mu)x}, \qquad \text{(B1)}
\end{aligned}$$

where we have used the expression for the Fourier coefficient from Eq. (17) and as before $V_{\mathrm{SB}}(x,t)$ is the potential of a single oscillating barrier. At this point we make use of the fact that we have restricted ourselves to setups in which the different Gaussian barriers have no significant overlap with one another. Hence we can exchange summation and integration and apply the coordinate transformation $\tilde{x} = x - x_{0,i}$ for each of the n_p integrals:

$$\begin{aligned}
V_{\mu\nu}^{(n)} &= \frac{1}{L}\sum_{s=1}^{n_p}\int_{-\infty}^{+\infty} dx\; V_{\mathrm{SB}}^{(n)}(x - x_{0,s}) e^{in(\omega t_0+\delta_s)} e^{i(2\pi/Ln_P)(\nu-\mu)x} \\
&= \frac{1}{L}\sum_{s=1}^{n_p}\int_{-\infty}^{+\infty} d\tilde{x}\; V_{\mathrm{SB}}^{(n)}(\tilde{x}) e^{in(\omega t_0+\delta_s)} e^{i(2\pi/Ln_P)(\nu-\mu)(\tilde{x}+x_{0,s})} \\
&= \sum_{s=1}^{n_p} V_{\mathrm{SB},\,\mu\nu}^{(n)} e^{i[n(\omega t_0+\delta_s)+(2\pi/Ln_p)(\nu-\mu)x_{0,s}]}. \qquad \text{(B2)}
\end{aligned}$$

APPENDIX C: SYMMETRY OF THE TIME EVOLUTION OPERATOR

First, we show that the symmetry given in Eq. (22) is equivalent to the relation

$$U_{\mu\nu}^{\kappa,j} = \left(U_{\mu\nu}^{-\kappa,-j}\right)^{\text{¤}} \qquad \text{(C1)}$$

for the matrix elements of the time evolution operator over the jth time step as given by Eq. (12) (we omit the dependence on the initial time t_0 for the sake of clarity) and we have adopted the notation $(U_{\mu\nu}^{\kappa,j})^{\Join} = U_{-\nu-\mu}^{\kappa,j}$ from [12]. As mentioned in the main text, the time evolution operator over an entire period of the driving is obtained as the product of the N operators $U_{\mu\nu}^{\kappa,j}$. For reasons of clarity, we will omit the momentum indices (μ,ν) for the time being. In analogy, the time evolution operator for the time interval (t_1,t_2) is given by

$$U^{\kappa}(t_2,t_1) = \prod_{j=j_1}^{j_2} U^{\kappa,j}, \tag{C2}$$

where j_1 and j_2 are the numbers of time steps corresponding to t_1 and t_2 and are given by $j_{1,2} = \lceil (N/T)t_{1,2} \rceil$. Now, if we assume that Eq. (C1) holds we find

$$\begin{aligned} U^{\kappa}(T-t_1,T-t_2) &= \prod_{j=N-j_2}^{N-j_1} U^{\kappa,j} = \prod_{j=j_2}^{j_1} U^{\kappa,N-j} \\ &= \prod_{j=j_2}^{j_1} (U^{-\kappa,j})^{\Join} = \left(\prod_{j=j_1}^{j_2} U^{-\kappa,j} \right)^{\Join} \\ &= [U^{-\kappa}(t_2,t_1)]^{\Join}. \end{aligned} \tag{C3}$$

Thus, the symmetry in Eq. (22) follows indeed from Eq. (C1). However, the validity of Eq. (C1) remains to be shown.

To make some progress we restrict ourselves to the first-order expansion of $U_{\mu\nu}^{\kappa,j}$ given by Eq. (12):

$$\begin{aligned} U_{\mu\nu}^{\kappa,j} &= \sum_{n=-\infty}^{+\infty} e^{in\omega j\Delta t} \left(\delta_{\mu\nu}\delta_{n0} + i\Delta t H_{\mu\nu}^{\kappa,(n)} \right) \\ &= \delta_{\mu\nu} + i\Delta t \sum_{n=-\infty}^{+\infty} e^{in\omega j\Delta t} H_{\mu\nu}^{\kappa,(n)}, \end{aligned} \tag{C4}$$

where we have used Eq. (A1) for the matrix elements of the Floquet operator $H_f(x,t)$. In comparison we obtain for $(U_{\mu\nu}^{-\kappa,-j})^{\Join}$

$$\begin{aligned} \left(U_{\mu\nu}^{-\kappa,-j}\right)^{\Join} &= U_{-\nu-\mu}^{-\kappa,-j} \\ &= \delta_{-\nu-\mu} + i\Delta t \sum_{n=-\infty}^{+\infty} e^{in\omega(-j)\Delta t} H_{-\nu-\mu}^{\kappa,(n)} \\ &= \delta_{\mu\nu} + i\Delta t \sum_{n=-\infty}^{+\infty} e^{in\omega j\Delta t} H_{-\nu-\mu}^{\kappa,(-n)} \\ &= \delta_{\mu\nu} + i\Delta t \sum_{n=-\infty}^{+\infty} e^{in\omega j\Delta t} H_{\mu\nu}^{\kappa,(n)} \\ &= U_{\mu\nu}^{\kappa,j}. \end{aligned} \tag{C5}$$

Here we exploited that $H_{-\nu-\mu}^{\kappa,(-n)} = H_{\mu\nu}^{\kappa,(n)}$, which follows directly from Eq. (15), as well as from the fact that the Fourier components of a time-reversal-symmetric function obey $V^{(n)}(x) = V^{(-n)}(x)$.

[1] P. Hänggi and F. Marchesoni, Rev. Mod. Phys. **81**, 387 (2009).
[2] P. Olbrich, E. L. Ivchenko, R. Ravash, T. Feil, S. D. Danilov, J. Allerdings, D. Weiss, D. Schuh, W. Wegscheider, and S. D. Ganichev, Phys. Rev. Lett. **103**, 090603 (2009).
[3] R. Gommers, S. Denisov, and F. Renzoni, Phys. Rev. Lett. **96**, 240604 (2006).
[4] P. Phoonthong, P. Douglas, A. Wickenbrock, and F. Renzoni, Phys. Rev. A **82**, 013406 (2010).
[5] A. Wickenbrock, P. C. Holz, N. A. Abdul Wahab, P. Phoonthong, D. Cubero, and F. Renzoni, Phys. Rev. Lett. **108**, 020603 (2012).
[6] T. Salger *et al.*, Science **326**, 1241 (2009)
[7] T. Salger, S. Kling, S. Denisov, A. V. Ponomarev, P. Hänggi, and M. Weitz, Phys. Rev. Lett. **110**, 135302 (2013).
[8] O. E. Alon, Phys. Rev. B **67**, 121103 (2003).
[9] S. Kohler, J. Lehmann, and P. Hänggi, Phys. Rep. **406**, 379 (2005).
[10] H. Schanz, M. F. Otto, R. Ketzmerick, and T. Dittrich, Phys. Rev. Lett. **87**, 070601 (2001).
[11] H. Schanz, T. Dittrich, and R. Ketzmerick, Phys. Rev. E **71**, 026228 (2005).
[12] S. Denisov, L. Morales-Molina, S. Flach, and P. Hänggi, Phys. Rev. A **75**, 063424 (2007).
[13] M. Grifoni, M. S. Ferreira, J. Peguiron, and J. B. Majer, Phys. Rev. Lett. **89**, 146801 (2002).
[14] G. G. Carlo, G. Benenti, and D. L. Shepelyansky, Phys. Rev. Lett. **95**, 164101 (2005).
[15] M. Heimsoth, C. E. Creffield, and F. Sols, Phys. Rev. A **82**, 023607 (2010).
[16] J. Gong, D. Poletti, and P. Hänggi, Phys. Rev. A **75**, 033602 (2007).
[17] S. Denisov, S. Flach, and P. Hänggi, Phys. Rep. **538**, 77 (2014).
[18] S. Denisov, L. Morales-Molina, and S. Flach, Europhys. Lett. **79**, 10007 (2007).
[19] F. Zhan, S. Denisov, A. V. Ponomarev, and P. Hänggi, Phys. Rev. A **84**, 043617 (2011).
[20] L. Morales-Molina, S. Flach, and J. B. Gong, Europhys. Lett. **83**, 40005 (2008).
[21] T. S. Monteiro, A. Rançon, and J. Ruostekoski, Phys. Rev. Lett. **102**, 014102 (2009).
[22] P. H. Jones, M. Goonasekera, D. R. Meacher, T. Jonckheere, and T. S. Monteiro, Phys. Rev. Lett. **98**, 073002 (2007).
[23] L. Chen, C. Xiong, H. C. Yuan, and L. H. Ding, Physica A **398**, 83 (2014).
[24] M. Sadgrove, T. Schell, K. Nakagawa, and S. Wimberger, Phys. Rev. A **87**, 013631 (2013).
[25] I. Dana, V. Ramareddy, I. Talukdar, and G. S. Summy, Phys. Rev. Lett. **100**, 024103 (2008).
[26] B. Liebchen, C. Petri, F. Lenz, and P. Schmelcher, Europhys. Lett. **94**, 40001 (2011).
[27] C. Petri, F. Lenz, B. Liebchen, F. K. Diakonos, and P. Schmelcher, Europhys. Lett. **95**, 30005 (2011).
[28] T. Wulf, C. Petri, B. Liebchen, and P. Schmelcher, Phys. Rev. E **86**, 016201 (2012).

[29] T. Wulf, B. Liebchen, and P. Schmelcher, Phys. Rev. Lett. **112**, 034101 (2014).
[30] C. Petri, F. Lenz, F. K. Diakonos, and P. Schmelcher, Phys. Rev. E **81**, 046219 (2010).
[31] B. Liebchen, F. K. Diakonos, and P. Schmelcher, New J. Phys. **14**, 103032 (2012).
[32] P. Reimann and M. Evstigneev, Europhys. Lett. **78**, 50004 (2007).
[33] T. Salger, G. Ritt, C. Geckeler, S. Kling, and M. Weitz, Phys. Rev. A **79**, 011605 (2009).
[34] K. Henderson, C. Ryu, C. MacCormick, and M. G. Boshier, New J. Phys. **11**, 043030 (2009).
[35] A. R. Kolovsky, S. Miyazaki, and R. Graham, Phys. Rev. E **49**, 70 (1994).
[36] J. H. Shirley, Phys. Rev. **138**, B979 (1965).
[37] D. J. Tannor, *Introduction to Quantum Mechanics: A Time-Dependent Perspective* (University Science Books, Sausalito, CA, 2007).
[38] F. H. M. Faisal and J. Z. Kamiński, Phys. Rev. A **56**, 748 (1997).
[39] H. Sambe, Phys. Rev. A **7**, 2203 (1973).
[40] R. Graham and J. Keymer, Phys. Rev. A **44**, 6281 (1991).
[41] K. Takahashi, Prog. Theor. Phys. Suppl. **98**, 109 (1985).
[42] J. von Neumann and E. Wigner, Phys. Z. **30**, 467 (1929).